Characteristics and evolution of plasma-jet-like structures in line-focused laser-produced plasmas

Zhi-zhan Xu

Center of Condensed Matter and Radiation Physics, China Center of Advanced Science and Technology (World Laboratory),
Beijing, People's Republic of China
*and Shanghai Institute of Optics and Fine Mechanics, Academia Sinica, P.O. Box 8211, Shanghai, People's Republic of China**

Shi-sheng Chen, Li-huang Lin, Zhi-ming Jiang, Wei-qing Zhang, and Ai-di Qian

Shanghai Institute of Optics and Fine Mechanics, Academia Sinica, P.O. Box 8211, Shanghai, People's Republic of China
(Received 18 March 1988)

We have used five-frame photography to investigate plasma-jet formation and its evolution in line-focused laser-produced plasmas. Small-scale plasma jets have been observed in low-Z and high-Z plasmas. We have also observed relatively large-scale plasma jets, which are similar in appearance to "tips of oxhorns" and always appear at the boundaries between hot plasma and cold target material or between two different-Z (e.g., high-Z and low-Z) plasmas. It is also shown that the plasma-jet structure is more pronounced for the short-wavelength-laser–irradiated targets. The causes of plasma jets and their influence on x-ray–laser schemes using a line-focused laser-produced plasma as a gain medium are discussed.

I. INTRODUCTION

In recent years, the approach of achieving extreme-ultraviolet (xuv) or x-ray lasing by using high-power lasers to produce and heat high-density plasmas has become very promising.[1-4] In this approach, a cylindrical lens is usually used in order to form a line-shaped plasma, which is necessary to obtain sufficient amplification of x-ray radiation along the focal line. The coupling characteristics of a line-focused laser with a plasma have a direct influence on the operating conditions for the plasma as a gain medium. However, nonuniformities such as plasma jets will be a serious problem for laser-pumped x-ray lasing research as they have been in laser fusion study. In the earlier experiment reported in Ref. 5, laser-produced plasmas at an irradiance on the target of 10^{13} W/cm^2 for a spot focus and 5×10^{11} W/cm^2 for a line focus were studied, but no plasma jets were observed. This was likely due to lower irradiances. Since then, plasma-jet structures have already been observed and were widely investigated in spot-focused laser-produced plasmas,[6-8] but relatively less in line-focused laser-produced plasmas.[9] In this paper, we report a detailed investigation of plasma-jet structures in experiments on line-focused lasers irradiating a variety of planar targets.

In previous experiments,[10] we have observed a line-focused laser beam break up into filaments. After the laser ceased to irradiate the target, we and others[9] have also observed small-scale plasma-jet-like structures in the underdense plasma. In recent experiments carried out at Shanghai Institute of Optics and Fine Mechanics (SIOM), we further investigated the coupling characteristics of a line-focused laser with plasmas. In these experiments, a five-frame optical-probing diagnostic system was used, which allows us to trace the evolution of the jet-like structures appearing in plasmas. We have observed not only the small-scale plasma jets and their evolution, but also relatively large-scale jet-like structures, which are similar in appearance to "tips of oxhorns" and always appear at the boundaries between hot plasma and cold target material or between two plasmas with different-Z materials (e.g., high Z and low Z). We have also used frequency-doubled laser light (530 nm) to irradiate targets. The results show that the plasma jets are more serious than those occurring in 1.06 μm laser-irradiated target experiments. The plasma jets could result in strong nonuniformities in the line-focused laser-produced plasmas and could eventually lead to gain spoiling in the operation of an x-ray laser using plasma as a gain medium.

II. EXPERIMENTAL SETUP

Figure 1 shows the layout of the experimental arrangement. In our experiments, two beams of the six-beam Nd-glass Laser Facility at SIOM (Ref. 11) are combined into one which is line focused on the targets. The focusing system consists of a cylindrical lens (planoconcave, with a 800–3000-mm radius of curvature) and an aspheric lens ($f/2$ with a 120-mm focal length). The resulting size of the focal line has a length of 1–4 mm and a width of 60–140 μm [full width at half maximum (FWHM)]. Sometimes, a large-size transverse width of the line focus is also used. The spatial uniformity of the line focus is acceptable in the axial direction, having at most local large-scale nonuniformities and an approximately Gaussian distribution in the transverse direction. The pulse width of the 1.06-μm laser is available from 200 to 800 ps (FWHM) and the energy of the prepulse is less than 10^{-6} of the main pulse. The output energy is in the range of 1–20 J, with corresponding average irradiance on the targets from 10^{12} to 10^{14} W/cm^2. Planar targets of different
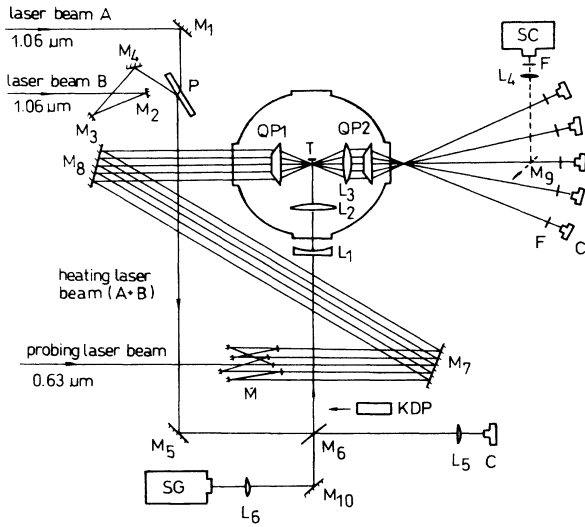
FIG. 1. Scheme of experimental arrangement. C, cameras; F, interference filters; KDP, frequency-doubling crystal; L_1, cylindrical lens; L_2 and L_3, aspheric lenses; L_4–L_6, convex lenses; M, five-beam splitting and optical delay; M_1–M_{10}, mirrors; P, polarizing plate; QP1 and QP2, quinque prisms; SC, streak camera; SG, spectrograph; T, target. Note that the x-ray detectors are not included in the diagram.

atomic-number materials (from low Z to high Z) and segmented targets consisted of two materials with different Z are used. In the experiments, a five-frame optical-probing diagnostic system is applied and will be described in Sec. III. The five-frame probing system can give us a time sequence of interferograms or shadowgrams showing the plasma evolution. In addition, we have also used other diagnostics in the experiments. These include TlAP crystal spectrographs for obtaining spatially resolved and integrated x-ray spectra, as well as an x-ray pinhole camera for obtaining images of x-ray emission of targets in the 1-keV range. Figure 2 shows the typical x-ray pinhole photographs of line-focused laser-produced plasmas from planar foil targets and segmented planar targets.

III. FIVE-FRAME OPTICAL PROBING DIAGNOSTIC SYSTEM

A. Probing pulse generation

The requirements of a probing beam for a laser-produced plasma are narrow pulsewidth, accurate sychronization with the main laser pulse, suitable wavelength, as well as no coincidence with self-generated harmonic emission from laser-produced plasmas. When we use one beam of the six-beam laser facility as the source to produce a probing pulse, the requirement of sychronization can be satisfied for these pulses coming originally from the same oscillator. The layout of the generation of the probing pulse is shown schematically in Fig. 3.[12] The 1.06-μm laser with energy of a few hundreds of a mJ is frequency doubled into 530 nm by a potassium dihydrogen phosphate (KDP) type-I crystal and frequency shift-
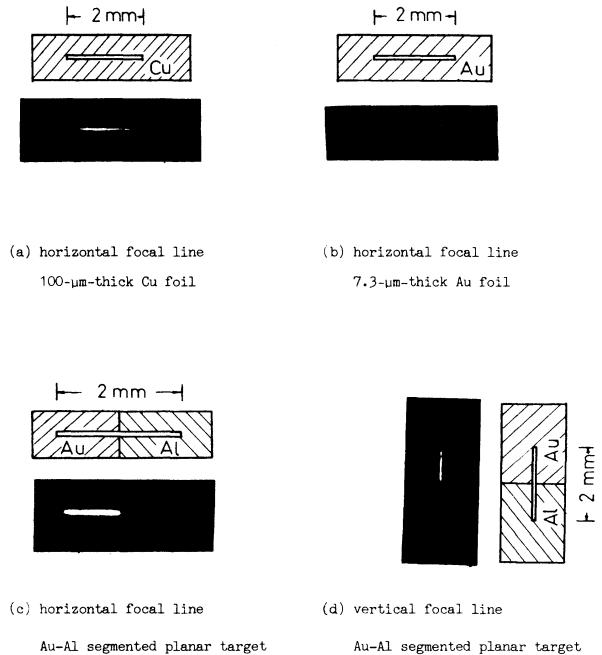

FIG. 2. Typical x-ray pinhole photographs of line-focused laser-produced plasmas. (a) Horizontal focal line, 100-μm-thick Cu foil; (b) horizontal focal line, 7.3-μm-thick Au foil; (c) horizontal focal line, Au-Al segmented planar target; (d) vertical focal line, Au-Al segmented planar target.

ed into 629.8 nm by stimulated Raman backscattering from dimethyl sulfoxide [$(CH_3)_2SO$] liquid so that the resulting probing beam does not interfere with the second harmonic emission from the laser-plasma interaction. Raman backscattering is used for better pulsewidth narrowing than that of the more generally used Raman forward scattering. In our case the pulsewidth of the probing pulse is about 50 ps while the corresponding pulsewidth of the 1.06-μm laser is about 250 ps, both are measured with a streak camera. The probing beam contains more than 200 μJ of light energy which ensures normal operation of the five-frame system.

B. Five-frame probing system

In order to get five plasma shadowgrams or interferograms at discrete times during the evolution of a laser-produced plasma, five individual probing pulses are re-
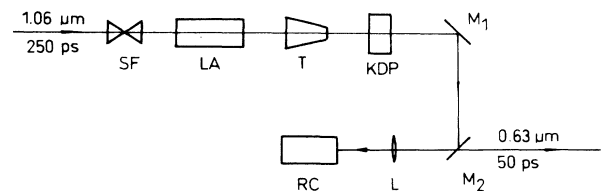

FIG. 3. Probing pulse generation using stimulated Raman backscattering. KDP, frequency-doubling crystal; L, convex lens; LA, laser amplifier; M_1 and M_2, dichroic mirrors; RC, Raman cell filled with dimethyl sulfoxide [$(CH_3)_2SO$]; SF, spatial filter; T, inverted telescope.
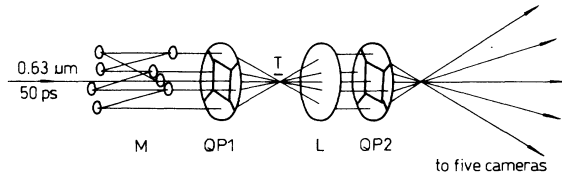
FIG. 4. Five-frame optical-probing diagnostic system. As a Wollaston prism and two polaroids are inserted, a five-frame interferometer of the Nomarski type can be set up conveniently. L, imaging lens; M, five-beam splitting and optical delay; QP1 and QP2, quinque prisms; T, target.

quired. As shown in Figs. 1 and 4, a multiplexer (M) is used to split the probing pulse into five individual pulses with approximately equal energy and spacing, as well as with adjustable optical delays between each other. Then a quinque prism (QP1) focuses them passing through the plasma, which is somewhat similar to that of Maaswinkel et al.[13] The orientation of these probing beams is arranged in a symmetrical form around the central one and
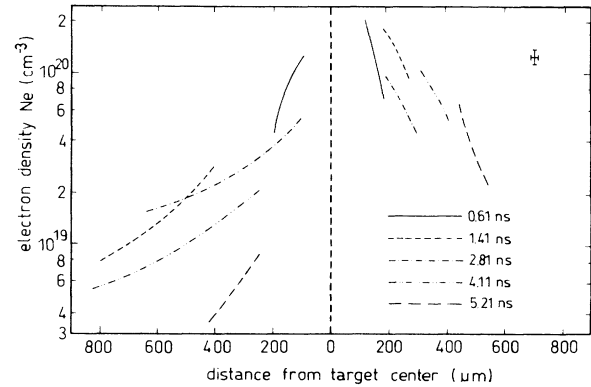
FIG. 6. On-axis plasma electron density distribution on both sides of the planar foil target deduced from Fig. 5 by the Abel inversion technique. Note the error bars are indicated on the above right. The laser is incident from the left to the right. The transverse coordinate indicates the distance from the target center.
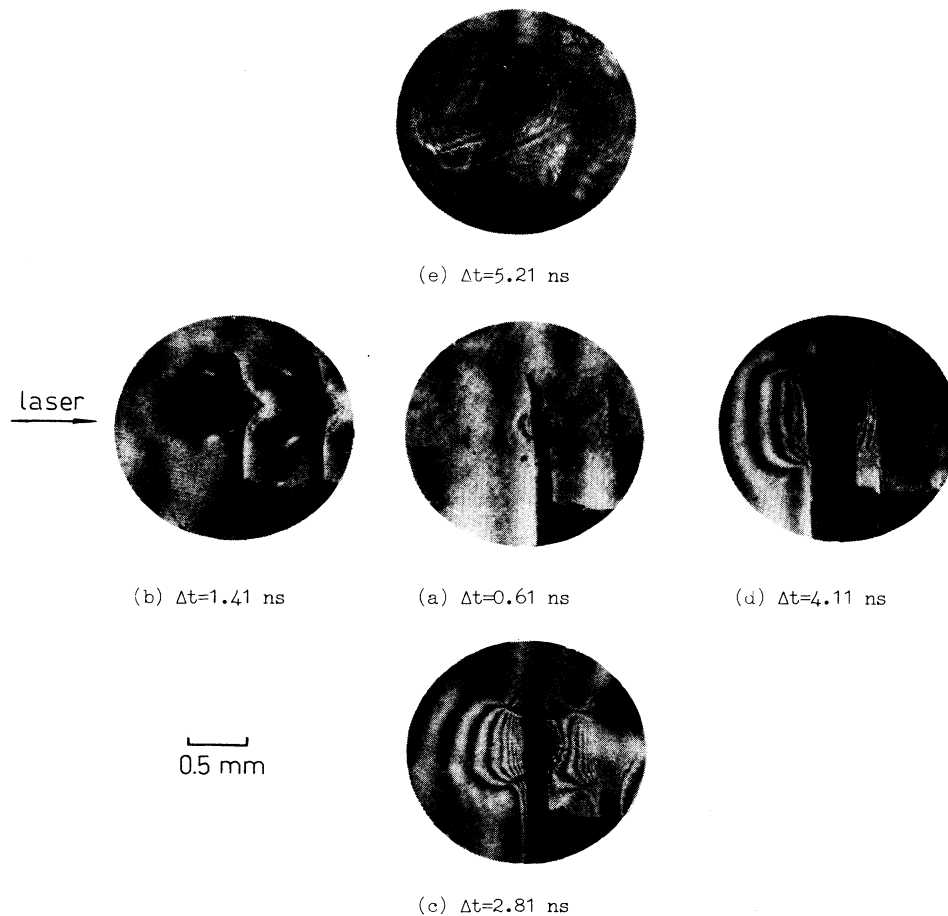

(e) Δt=5.21 ns

(b) Δt=1.41 ns   (a) Δt=0.61 ns   (d) Δt=4.11 ns

(c) Δt=2.81 ns

FIG. 5. Typical sequence of interferograms obtained by the five-frame photography showing the plasma evolution. The target is a 10-μm-thick Co foil and is irradiated by a spot-focused 1.06-μm laser light (from the left to the right). Δt is the delay time relative to the peak of the laser pulse. Note that five probing beams traverse the plasma in a direction perpendicular [for (a), (c), and (e)] or nearly perpendicular [for (b) and (d)] to the target surface normal.
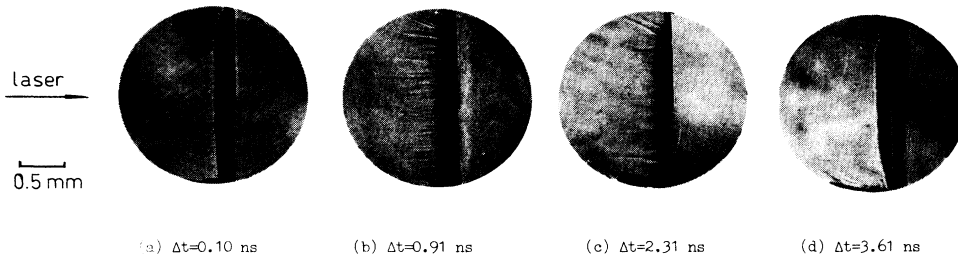
(a) Δt=0.10 ns   (b) Δt=0.91 ns   (c) Δt=2.31 ns   (d) Δt=3.61 ns

FIG. 7. Sequence of shadowgrams showing plasma jets and their time evolution. The 100-μm-thick Al planar foil target is irradiated by a line-focused laser light at an irradiance of 3.5×10^{13} W/cm^2. The probing beams are orthogonal to the 2-mm-long focal line.

with a slight angle to each other. They traverse the plasma in the direction perpendicular or nearly perpendicular to the heating laser axis, so as to produce five side-view photographs. The imaging system consists of a prism (QP2) and a lens so that it can produce five spatially separated shadowgrams, or interferograms when an interferometer of the Nomarski type[14] is inserted. Time delays between the probing pulses and the heating pulse are adjustable and can be measured with a streak camera within an accuracy of 50 ps. The spatial resolution of this system is less than 5 μm while the temporal resolution is determined by the probing pulsewidth.

A set of interferograms showing the evolution of a spot-focused laser-produced plasma, obtained by using the five-frame system, is shown in Fig. 5. The corresponding plasma on-axis density distributions are shown in Fig. 6, which are obtained by Abel inversion technique. By comparing these density distributions to the results of computer calculations, we can get very useful

information such as energy absorption, energy transport in the plasma, etc.

IV. DESCRIPTION OF THE EXPERIMENTAL INVESTIGATIONS

A. Small-scale plasma jets

In the experiments on observing plasma-jet structure in line-shaped plasmas, two different pulsewidths (FWHM) of 250 and 700 ps are used. As described before, the heating laser is made of two individual laser beams with 200–400 ps pulsewidth, respectively. The delay time between them is adjustable so the desired pulsewidth can be obtained. In our long pulse experiments, a combined laser pulse of about 700 ps (FWHM) is set.

Figure 7 shows the time evolution of the plasma jets in the coronal plasma, whose electron density is in the range $10^{18} - 10^{20}$ cm^{-3}, for an Al foil target irradiated by a line-focused laser with 3.5×10^{13} W/cm^2 at 250 ps (FWHM).

before shot

laser

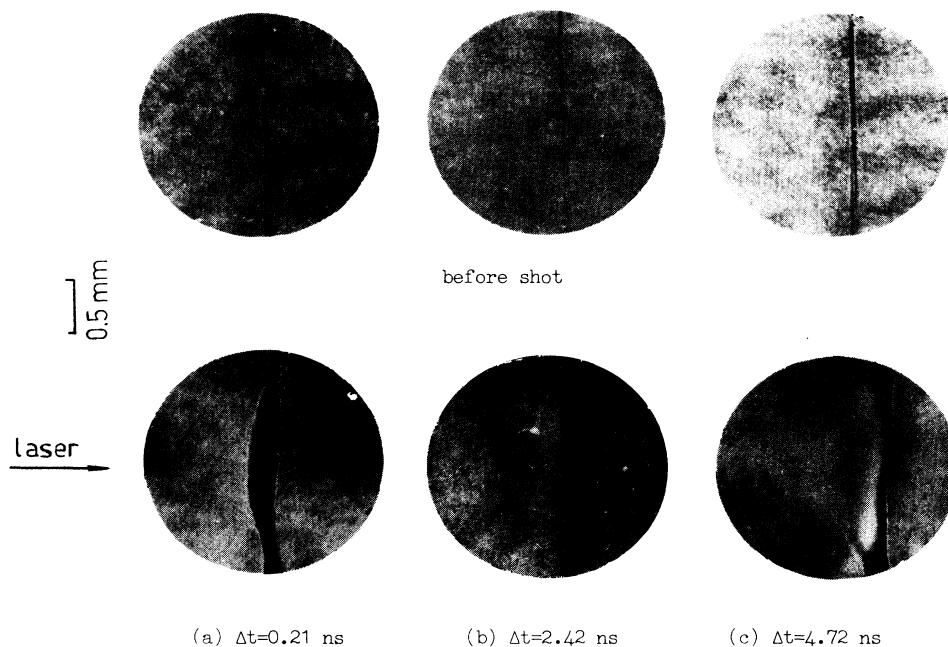(a) Δt=0.21 ns   (b) Δt=2.42 ns   (c) Δt=4.72 ns

FIG. 8. Sequence of shadowgrams showing plasma jets appearing in a long-pulse laser experiment in which a 1.2-μm-thick Cu target is used. The line-focused laser light has a FWHM of 700 ps and an irradiance of 9×10^{13} W/cm^2. Note that the upper shadowgrams shown in the figure are the relevant static pictures and the probing beams are orthogonal to the 1-mm-long focal line.

When at $\Delta t = 0.1$ ns (i.e., the arrival time of the peak of the probing pulse on the plasma is 0.1 ns later than that of the heating laser pulse), plasma jets with a short length expanding normally to the planar-target surface can be seen. After the laser ceases to heat the target, as shown in Figs. 7(b) ($\Delta t = 0.91$ ns) and 7(c) ($\Delta t = 2.4$ ns), the plasma jets grow more rapidly with time and the underdense plasma is broken into a number of jets with an average expanding velocity of 1.0×10^7 cm/s, which is about five times than that of the bulk plasma, and the transverse spatial scale is $10-30$ μm. Then the jets will collapse and evanesce gradually by some smoothing mechanisms[15] (e.g., thermal-conductive effect), see Fig. 7(d).

In long-pulse (about 700 ps FWHM) experiments, similar plasma-jet structure and its time evolution are also observed. As shown in Fig. 8 for a Cu foil target irradiated by a line-focused laser light at an intensity of 9.0×10^{13} W/cm^2, we can see that at $\Delta t = 0.2$ ns distinct jets have not appeared in the coronal plasma. However, the plasma jets are pronounced after the end of the heating laser pulse, e.g., at $\Delta t = 2.4$ ns.

Although various mechanisms may be responsible for the occurrence of the plasma jets, the characteristics of their time evolution indicate that the jets are initially formed during the laser heating pulse which suggests that they may be due to a combination of filamentation of the laser beam and certain plasma instabilities.[16,17] In this period, the instabilities may be excited, but they can grow still rapidly even after the laser ceases to irradiate the target, which make the coronal plasma break up into a lot of small-scale jets. Later, some smoothing mechanisms[15] will be dominant and make the instabilities saturate. Eventually the jet structure tends to collapse or evanesce.

B. Plasma jets like "tips of oxhorns"

In addition to the small-scale plasma jets described above, we have also observed relatively large-scale plasma-jet structure, which is similar in appearance to "tips of oxhorns."

Figure 9 shows an interferogram and a shadowgram

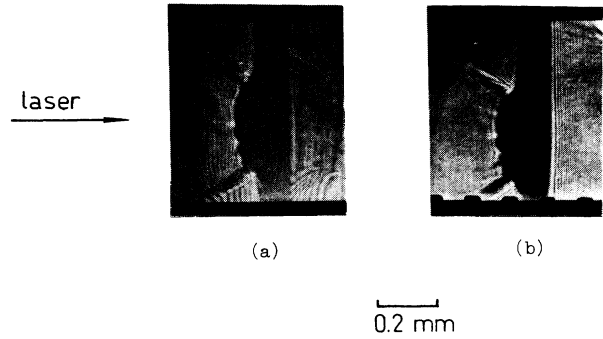(a)   (b)

0.2 mm

FIG. 9. (a) Interferogram and (b) shadowgram showing the relatively large-scale plasma-jet-like structure are recorded simultaneously by two-frame photography at $\Delta t = 2.9$ ns. The target is a 100-μm-thick Al foil and is irradiated by a line-focused laser light (with a horizontal focal line) at an irradiance of 1.4×10^{13} W/cm^2. The probing beam is parallel to the focal line. Note that the plasma jets shown in the figure are similar in appearance to "tips of oxhorns."

which are photographed simultaneously in one shot by a two-frame photography. The probing beam is parallel to the focal line and the Al target is irradiated at an irradiance of 1.4×10^{13} W/cm^2. The large-scale plasma jets are symmetrical about the focal line, like a pair of "tips of oxhorns." The interferogram indicates that the densities in the jets are higher than that of the ambient plasma. These jets always appear at the boundary between the hot plasma and the cold solid target material. The tips of the plasma jets tend to the side of the cold target material, and have an angle of $60°-65°$ with respect to the target surface, which hardly changes with the target atomic number Z and the laser-light irradiance on the target.

In order to clarify whether the refraction effect of the probing beam passing through the plasma causes the above-mentioned jet structure, a special laser-irradiating method is used, as shown in Fig. 10. The laser line focus lies horizontally on the Cu planar target such that its upper portion falls into the vacuum. The shadowgrams
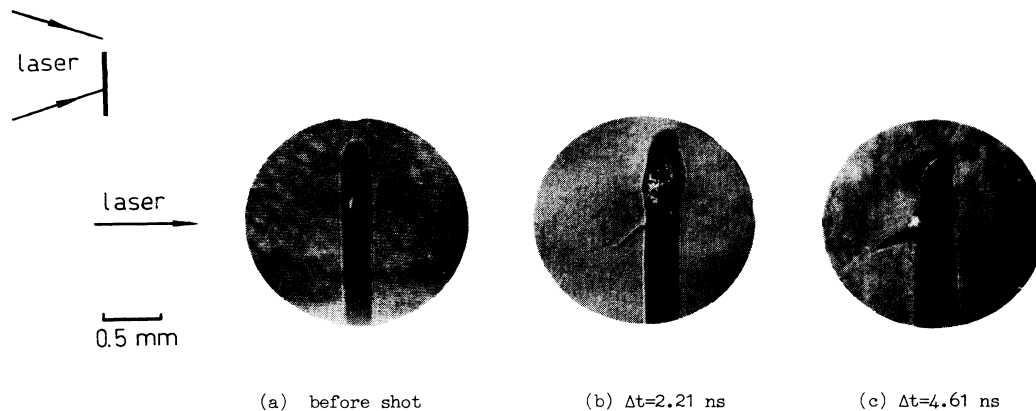

(a) before shot   (b) $\Delta t=2.21$ ns   (c) $\Delta t=4.61$ ns

FIG. 10. Shadowgrams showing the plasma jet similar in appearance to "tips of oxhorns," which appears only at the boundary between the hot plasma and the cold target material. The target is a 100-μm-thick Cu foil and is irradiated by a line-focused laser (with a horizontal focal line) at an irradiance of 4×10^{12} W/cm^2. The probing beam is parallel to the focal line. Note that the laser focus is located such that its upper portion falls into the vacuum (see the sketch on the above left).

showing the plasma jet and its evolution in this special irradiation case are also shown in Fig. 10, which are recorded by the five-frame diagnostic system. At $\Delta t = 2.1$ ns, a plasma jet appears in the lower part of the target, i.e., at the boundary between the hot plasma and the cold target material. Then this jet grows with time, which is similar in appearance to the tip of an oxhorn, and becomes much more pronounced at $\Delta t = 4.6$ ns, like those shown in Fig. 9. Nevertheless, this jet does not appear in the upper part of the target near the vacuum throughout. It seems that the interaction between the hot plasma and the cold target material is one of the causes of the "tips of oxhorns" jet structure.

The "tips of oxhorns" jets appear not only at the boundary between the hot plasma and the cold solid target material, but also appear at the boundary between two different-Z (e.g., Au-Al) plasmas. As shown in Fig. 11, a segmented target (Au-Al) is irradiated by a line-focused laser light at an irradiance of 1.0×10^{13} W/cm^2. The focal line is orthogonal to the boundary and is located such that the upper half irradiates the Al part and the lower half irradiates the Au part. The shadowgram taken at $\Delta t = 0.9$ ns shows that a jet exists at the boundary between two different-Z plasmas, whose tip tends to the Al plasma.

These jets, similar in appearance to "tips of oxhorns" at the boundaries, appear and grow up with time not only after the end of the heating laser pulse, but also in the edge region of the plasma beyond the laser focal region, which is formed by thermal conduction. The nonuniformities of the incident heating laser beam is less likely to be the cause for these jet structures. At the boundaries between the hot plasma and the cold solid target, or between two plasmas with different-Z numbers, there are large temperature and density gradients, so the large heat flow may occur. Therefore, the electronthermal and magnetothermal instabilities due to the occurrence of the
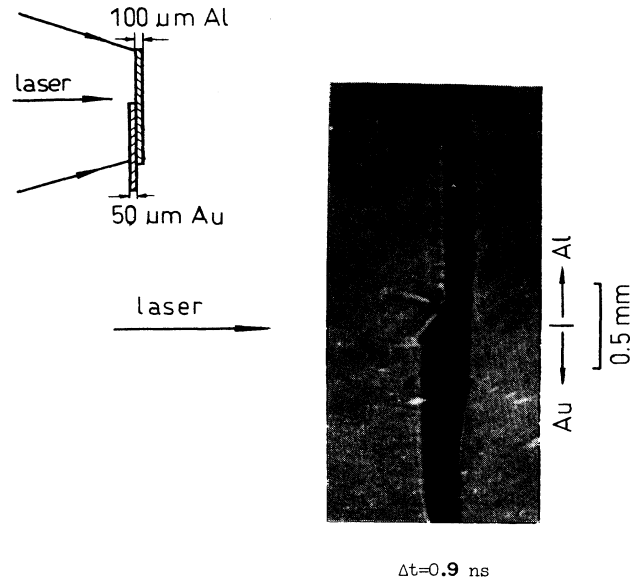

At=0.9 ns

FIG. 11. Shadowgram showing plasma jet similar in appearance to "tip of oxhorn," which appears at the boundary between two plasmas with different materials (Au, Al). The Au-Al segmented planar target (see the sketch on the above left) is used and irradiated by a 2-mm-long line-focused laser light at an irradiance of 1.0×10^{13} W/cm^2. Note that the line focus is located such that the upper half irradiates the Al part and the lower half irradiates the Au part.

heat flows may be excited and grow up, eventually producing plasma jet structures.[16]

C. Plasma jets in the frequency-doubled (0.53-μm) laser irradiation

We have also carried preliminary experiments on the frequency-doubled (0.53-μm) laser-irradiated targets.

(a) 100-μm-thick Cu target

(a) Δt=0.91 ns   (b) Δt=2.21 ns   (c) Δt=3.61 ns   (d) Δt=4.61 ns
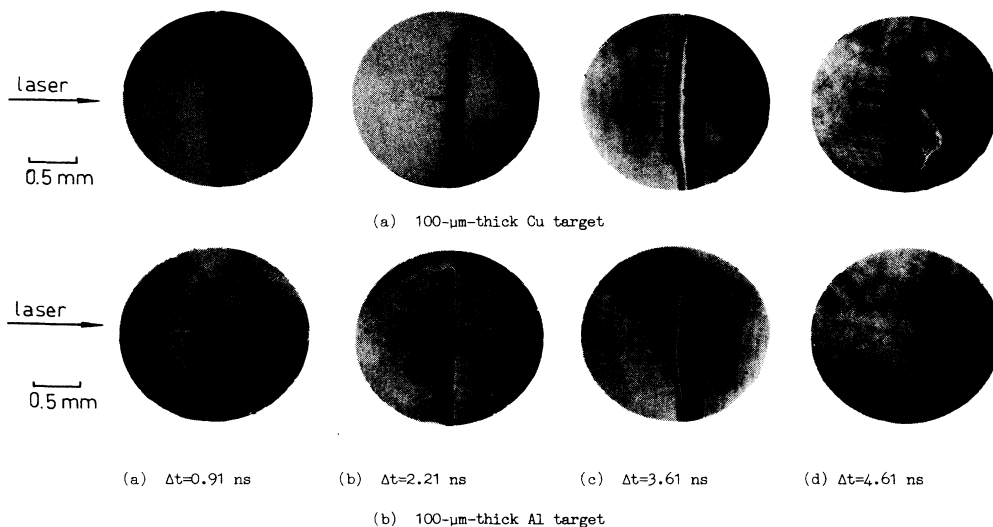
(b) 100-μm-thick Al target

FIG. 12. Two sequences of shadowgrams showing plasma jets and their time evolution for (a) 100-μm-thick Cu and (b) Al planar foil targets irradiated with spot-focused, frequency-doubled (0.53-μm) laser lights at an irradiance of 3×10^{12} W/cm^2. Note that here large focal spots are chosen.

Figure 12 shows the shadowgrams of Cu [Fig. 12(a)] and Al [Fig. 12(b)] planar foil targets irradiated by 0.53-μm spot-focused laser light. At $\Delta t = 0.91$ ns, the underdense plasmas has broken into a number of jets with transverse dimension in the Cu plasma smaller than that in the Al plasma. The variation of the on-axis length of the plasma jets with time, deduced from Fig. 12, is shown in Fig. 13. Initially, the plasma jets develop rapidly with time in the Al plasma. But the growth is saturated when $\Delta t \sim 3$ ns. In contrast with the Al plasma, the jets in the Cu plasma develop relatively slowly and the growth is not saturated even for $\Delta t \sim 4$ ns.

The different jet evolution characteristics in the Al and Cu plasmas suggest that the electron thermal conduction has great influence on the jet evolution. When the jets are formed in the plasma, thermal conduction tends towards smoothing these nonuniform structures. Thus, although the plasma jets grow rapidly in a low-Z plasma, they will also be smoothed faster because of the large thermal conductivity. In addition, compared with the results of 1.06-μm laser-irradiated targets, our experimental results have shown that the growth of the plasma jets is more pronounced in 0.53-μm laser experiments at the same irradiance (see Fig. 7). It may be because of the poor thermal smoothing ability for the 0.53-μm laser-produced plasmas.

V. DISCUSSION

We have used the five-frame photography to investigate plasma-jet formation and its evolution in line-focused laser-produced plasmas. Small-scale plasma jets appearing in low- and high-Z plasmas have been observed. We have also observed relatively large-scale plasma jets, which are similar in appearance to "tips of ox-horns" and always appear at the boundaries between the hot plasma and the cold target material, or between two different-Z plasmas. It is also shown that the plasma-jet structure is more pronounced for the short-wavelength laser-irradiated targets.

Laser-beam filamentation and plasma-jet formation would have detrimental effects on the operation of an x-ray laser using a line-focused laser-produced plasma as a gain medium, since the expected uniform plasma state would be destroyed. The self-focusing and filamentation of a laser beam originate from the direct interaction between the laser and plasma, and conversely have great influence on the characteristics of the interactions and the state of the resultant plasma. However, plasma jets caused by certain plasma instabilities can be formed during the laser heating pulse, and develop more rapidly with time after the end of the heating laser pulse.[8,9] The plasma jets and the laser-beam filamentation can couple
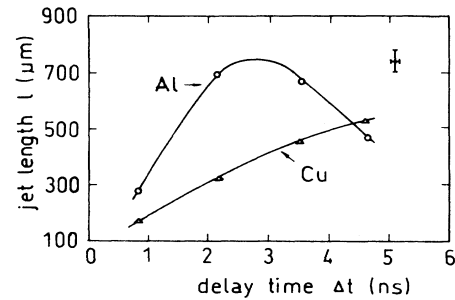

FIG. 13. Variation of on-axis length l of plasma jet with the delay time Δt deduced from Fig. 12. Note that there is a distinct saturated region for an Al target. The typical error bars are indicated on the above right.

or affect each other, then strengthen the nonuniformities in a laser-produced plasma. The effects of plasma jets are manifold. Firstly, if early enough, plasma jets could provide an initial density fluctuation to trigger laser filamentation. Secondly, strong nonuniformities in the plasma result from these jet structures. Finally, these nonuniformities may induce hydrodynamic turbulence and other unexpected nonlinear effects, which would reduce the x-ray gain significantly. For example, the expected uniform plasma state with suitable density and temperature would not be formed. Griem[18] has pointed that the hydrodynamic turbulence in a plasma would lead to a large reduction in calculated average gains when the turbulence wavelength is below a critical size. The plasma-jet formation may be an original source of the plasma turbulence with small wavelength, then result in gain spoiling. It should also be indicated that in the recombination pumping scheme, significant recombination which results in x-ray lasing is generally formed after the end of the laser heating pulse,[19] when the plasma jets will become much more pronounced. Therefore the plasma jets might become a serious obstacle in achieving optimum x-ray lasing in the type of experiments using a line-focused laser-produced plasma as a gain medium. It can be expected that with the development of x-ray laser research, people will pay more attention to the formation mechanisms and the suppressing methods of the plasma-jet structures in line-focused laser-irradiated targets.

ACKNOWLEDGMENTS

---

*Address for correspondence.

[1]D. L. Matthews, P. L. Hagelstein, M. D. Rosen, M. J. Eckart, N. M. Ceglio, A. U. Hazi, H. Medecki, B. J. MacGowan, J. E. Trebes, B. L. Whitten, E. M. Campbell, C. W. Hatcher, A. M. Hawrylik, R. L. Kauffman, L. D. Pleasance, G. Rambach, J. H. Scofield, G. Stone, and T. A. Weaver, Phys. Rev. Lett. 54,

110 (1985).

[2]M. D. Rosen, P. L. Hagelstein, D. L. Matthews, E. M. Campbell, A. U. Hazi, B. L. Whitten, B. J. MacGowan, R. E. Turner, R. W. Lee, G. Charatis, C. E. Busch, C. L. Shepard, and P. D. Rockett, Phys. Rev. Lett. 54, 106 (1985).

[3]J. F. Seely, C. M. Brown, U. Feldman, M. Richardson, B.

Yaacobi, and W. E. Behring, Opt. Commun. **54**, 289 (1985).

[4]M. C. Richardson, Bull. Am. Phys. Soc. **30**, 1801 (1985).

[5]J. F. Reintjes, T. N. Lee, R. C. Eckardt, and R. A. Andrews, J. Appl. Phys. **47**, 4457 (1976).

[6]G. Thiell and B. Meyer, Laser Part. Beams **3**, 51 (1985).

[7]J. A. Stamper, S. H. Gold, S. P. Obenschain, E. A. Mclean, and L. Sica, J. Appl. Phys. **52**, 6562 (1981).

[8]O. Willi, P. T. Rumsby, and S. Sartang, IEEE J. Quantum Electron. **QE-17**, 1909 (1981).

[9]M. D. Burgess, R. Dragila, B. Luther-Davies, K. A. Nugent, A. J. Perry, G. J. Tallents, M. G. Richardson, and R. S. Craxton, Phys. Rev. A **32**, 2899 (1985).

[10]Zhi-zhan Xu, P. H. Y. Lee, Li-huang Lin, Wei-qing Zhang, Zhi-ming Jiang, Shao-xian Meng, Jia-jin Yu, and Ai-di Qian, Opt. Commun. **61**, 199 (1987).

[11]Zhi-zhan Xu, An-ming Li, Shi-sheng Chen, Li-huang Lin, Xiang-chun Liang, Pin Ouyang, Guang-yu Yin, and Shin-fa

Hou, Chin. Phys. **1**, 548 (1981).

[12]Zhi-ming Jiang, Shao-xian Meng, Wei-qing Zhang, Li-huang Lin and Zhi-zhan Xu, Nucl. Fusion Plasma Phys. **7**, 127 (1987) (in Chinese).

[13]A. G. M. Maaswinkel, R. Sigel, H. Baumhacker, and G. Brederlow, Rev. Sci. Instrum. **55**, 48 (1984).

[14]R. Banattar, C. Povics, and R. Sigel, Rev. Sci. Instrum. **50**, 1583 (1979).

[15]W. C. Mead and J. D. Lindl, University of California Report No. UCLA-78549, 1976 (unpublished); Bull. Am. Phys. Soc. **21**, 1102 (1976).

[16]H. G. Hains, Phys. Rev. Lett. **28**, 917 (1981).

[17]R. G. Evans, J. Phys. D **28**, L173 (1981).

[18]H. R. Griem, Phys. Rev. A **33**, 3580 (1986).

[19]G. J. Pert, in *Laser-Plasma Interactions 3, Scottish Universities Summer School in Physics, 1985,* edited by M. B. Hooper (unpublished), p. 315.
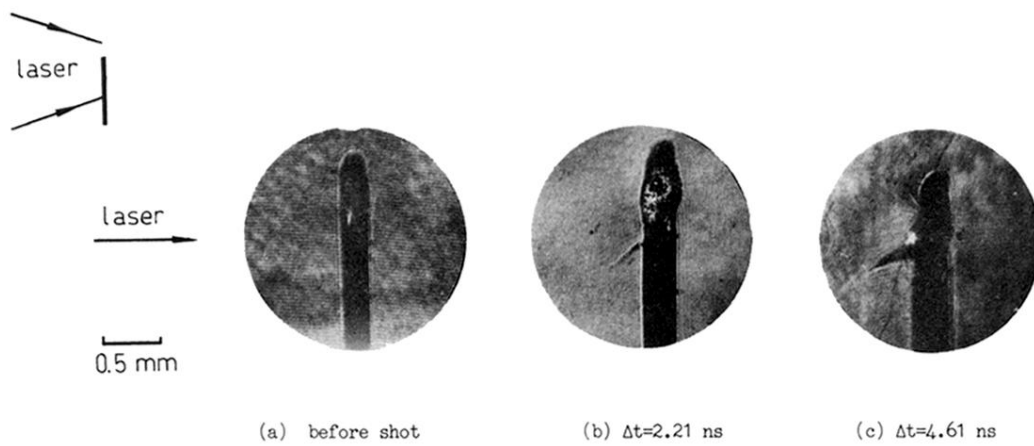
FIG. 10. Shadowgrams showing the plasma jet similar in appearance to "tips of oxhorns," which appears only at the boundary between the hot plasma and the cold target material. The target is a 100-μm-thick Cu foil and is irradiated by a line-focused laser (with a horizontal focal line) at an irradiance of 4×10^{12} W/cm^2. The probing beam is parallel to the focal line. Note that the laser focus is located such that its upper portion falls into the vacuum (see the sketch on the above left).

100 μm Al

laser

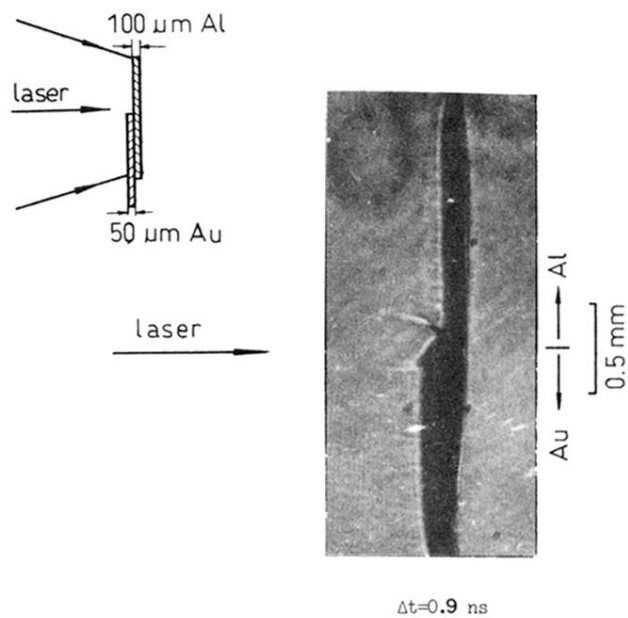50 μm Au

laser

Al

0.5 mm

Au

Δt=0.9 ns

FIG. 11. Shadowgram showing plasma jet similar in appearance to "tip of oxhorn," which appears at the boundary between two plasmas with different materials (Au, Al). The Au-Al segmented planar target (see the sketch on the above left) is used and irradiated by a 2-mm-long line-focused laser light at an irradiance of 1.0×10^{13} W/cm^2. Note that the line focus is located such that the upper half irradiates the Al part and the lower half irradiates the Au part.

laser →

0.5 mm

(a)   100-μm-thick Cu target

laser →

0.5 mm

(a)   Δt=0.91 ns   (b)   Δt=2.21 ns   (c)   Δt=3.61 ns   (d)   Δt=4.61 ns
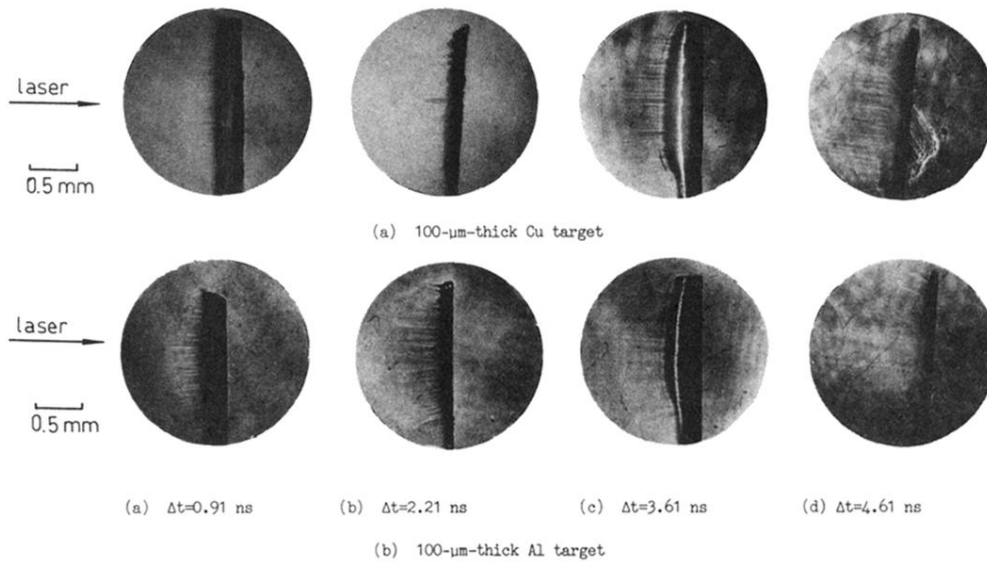
(b)   100-μm-thick Al target

FIG. 12. Two sequences of shadowgrams showing plasma jets and their time evolution for (a) 100-μm-thick Cu and (b) Al planar foil targets irradiated with spot-focused, frequency-doubled (0.53-μm) laser lights at an irradiance of 3×10^{12} W/cm^2. Note that here large focal spots are chosen.

(e) Δt=5.21 ns

laser →

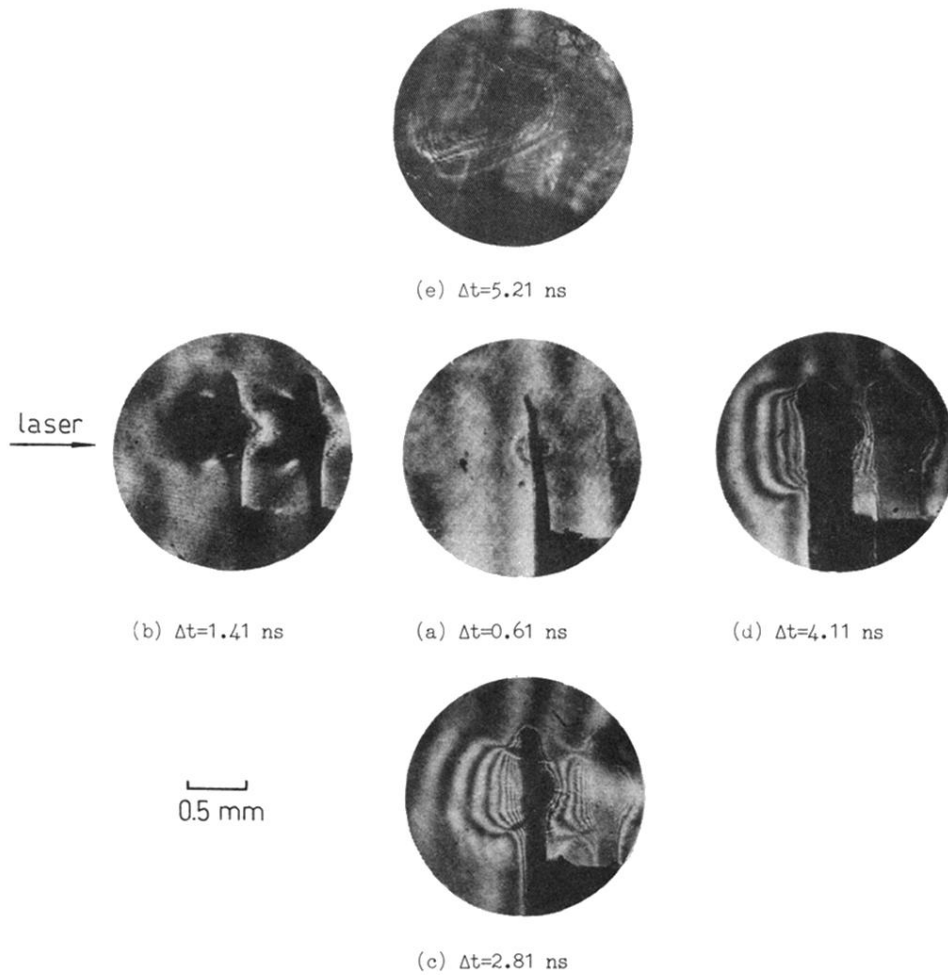(b) Δt=1.41 ns   (a) Δt=0.61 ns   (d) Δt=4.11 ns

0.5 mm

(c) Δt=2.81 ns

FIG. 5. Typical sequence of interferograms obtained by the five-frame photography showing the plasma evolution. The target is a 10-μm-thick Co foil and is irradiated by a spot-focused 1.06-μm laser light (from the left to the right). Δt is the delay time relative to the peak of the laser pulse. Note that five probing beams traverse the plasma in a direction perpendicular [for (a), (c), and (e)] or nearly perpendicular [for (b) and (d)] to the target surface normal.
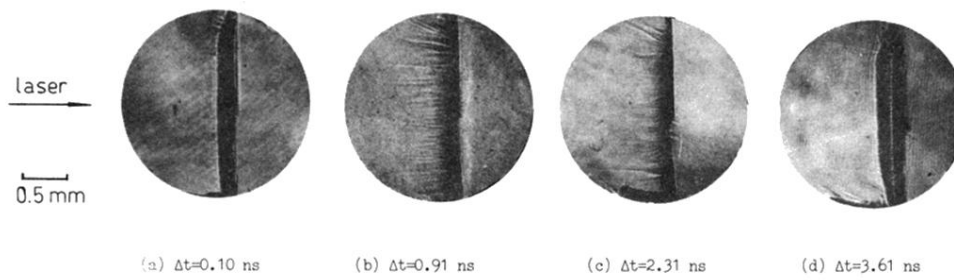
laser →

0.5 mm

(a) Δt=0.10 ns   (b) Δt=0.91 ns   (c) Δt=2.31 ns   (d) Δt=3.61 ns

FIG. 7. Sequence of shadowgrams showing plasma jets and their time evolution. The 100-μm-thick Al planar foil target is irradiated by a line-focused laser light at an irradiance of 3.5×10^{13} W/cm^2. The probing beams are orthogonal to the 2-mm-long focal line.
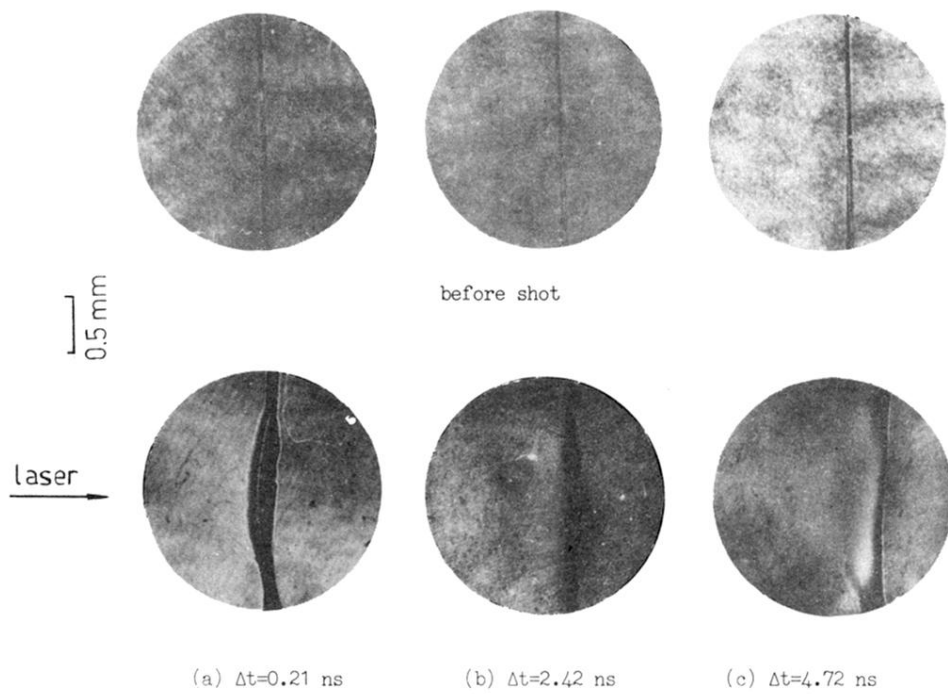
0.5 mm

laser →

before shot

(a) Δt=0.21 ns   (b) Δt=2.42 ns   (c) Δt=4.72 ns

FIG. 8. Sequence of shadowgrams showing plasma jets appearing in a long-pulse laser experiment in which a 1.2-μm-thick Cu target is used. The line-focused laser light has a FWHM of 700 ps and an irradiance of 9×10^{13} W/cm^2. Note that the upper shadowgrams shown in the figure are the relevant static pictures and the probing beams are orthogonal to the 1-mm-long focal line.
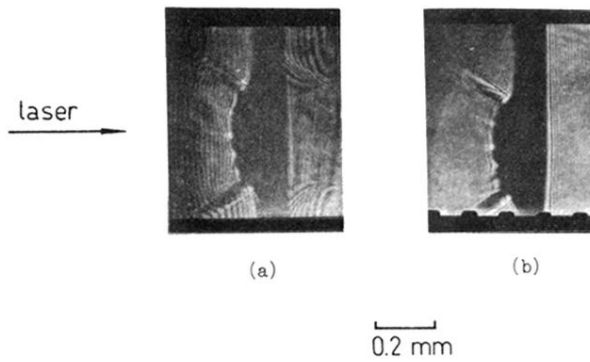
laser →

(a)   (b)

|—————| 0.2 mm

FIG. 9. (a) Interferogram and (b) shadowgram showing the relatively large-scale plasma-jet-like structure are recorded simultaneously by two-frame photography at $\Delta t = 2.9$ ns. The target is a 100-μm-thick Al foil and is irradiated by a line-focused laser light (with a horizontal focal line) at an irradiance of 1.4×10^{13} W/cm^2. The probing beam is parallel to the focal line. Note that the plasma jets shown in the figure are similar in appearance to "tips of oxhorns."